

Analyzing the frequency shift of physisorbed CO₂ in metal organic framework materials

Yanpeng Yao,¹ Nour Nijem,² Jing Li,³ Yves J. Chabal,² David C. Langreth,¹ and T. Thonhauser⁴

¹*Department of Physics and Astronomy, Rutgers University, Piscataway, New Jersey 08854, USA*

²*Department of Materials Science and Engineering,
University of Texas at Dallas, Richardson, Texas 75080, USA*

³*Department of Chemistry and Chemical Biology,
Rutgers University, Piscataway, New Jersey 08854, USA*

⁴*Department of Physics, Wake Forest University, Winston-Salem, North Carolina 27109, USA*

(Dated: August 20, 2018)

Combining first-principles density functional theory simulations with IR and Raman experiments, we determine the frequency shift of vibrational modes of CO₂ when physisorbed in the iso-structural metal organic framework materials Mg-MOF74 and Zn-MOF74. Surprisingly, we find that the resulting change in shift is rather different for these two systems and we elucidate possible reasons. We explicitly consider three factors responsible for the frequency shift through physisorption, namely (i) the change in the molecule length, (ii) the asymmetric distortion of the CO₂ molecule, and (iii) the direct influence of the metal center. The influence of each factor is evaluated separately through different geometry considerations, providing a fundamental understanding of the frequency shifts observed experimentally.

PACS numbers: 68.43.Bc, 68.43.Fg, 84.60.Ve

I. INTRODUCTION

physisorption of small molecules in multi-porous materials such as zeolites and metal organic framework (MOF) materials has experienced a surge of interest due to its potential for hydrogen-storage and gas-separation applications.^{1–30} MOF structures have been widely investigated in order to find faster absorption and higher storage densities, as well as proper binding energies.^{4–30} In order to design new MOFs with improved properties, it is of critical importance to understand the nature of the interaction between the absorbed molecule and the MOF host. Such understanding can either be gained through theory, using first-principles simulations,^{8–18} or through experimental probes, such as infrared (IR) absorption and Raman scattering.^{8–11,18,20–24}

Much progress has been made in improving the properties of MOFs. For example, it has been shown that using unsaturated metal centers, such as MOF74 with open Mg, Mn, Zn, Ni, Cu, or HKUST-1 with Cu, results in higher absorption density for hydrogen and faster absorption at small partial CO₂ pressures, the latter of which is highly desirable for CO₂ capturing applications.^{5–9,14–17,19–22} It has further been shown that iso-structural MOFs with different open metal centers can have very different absorption rates at low pressure.⁷ In particular, the electronically similar metal centers Mg and Zn result in a much faster CO₂ uptake rate in Mg-MOF74 than in Zn-MOF74 at a pressure smaller than 0.1 atm.⁷ However, when previous research yields contradictory results, it becomes difficult to gain further insight; e.g. while the frequency shift of the asymmetric stretch mode of absorbed CO₂ in Mg-MOF74 has been reported to be blue shifted in one work using IR spectra and B3LYP-D* calculation,¹⁰ it was reported

as a red shift in another work using density functional theory (DFT) with local density approximation (LDA) simulations.⁸ Furthermore, a clear correlation between the frequency shifts of the absorbed molecules and other absorption properties such as the binding energy or the adsorption site is still missing, which makes it difficult to directly correlate the observed results with the physical nature of the absorption process.

Van der Waals density functional theory^{31–33} (vdW-DF2) can be used as a very effective tool to understand the molecule/MOF interactions. Unlike previous simulations using LDA or GGA⁸ where long-range van der Waals interactions are not included consistently, or B3LYP-D*¹⁰ where the empirical parameters are used to incorporate the long-range dispersion terms, in our vdW-DF2 method, the exchange-correlation functional includes the—for these systems so important—long-range van der Waals interactions between the MOF structure and the physisorbed CO₂ molecules in a seamless³² and fully self consistent way.³³ vdW-DF2 and its predecessor vdW-DF have been successfully applied to many van der Waals systems,³⁴ ranging from simple dimers³⁵ and physisorbed molecules³⁶ to DNA and drug design.³⁷ In particular, it has been demonstrated that vdW-DF2 can correctly capture the interaction and determine the adsorption sites, binding energy, and vibrational frequencies for small molecules absorbed in different MOFs.^{9,11–13}

To resolve the contradicting results in literature, and to achieve a better understanding of the physics that determines the frequency shift of the absorbed molecule, in this work we combine both theoretical first-principles electronic-structure simulation using vdW-DF2 and experimental IR and Raman spectroscopy to study the CO₂ absorption in the iso-structural MOFs Mg-MOF74 and

Zn-MOF74. In the first step, we use our experimental probes to determine the absorption behavior and the vibrational frequencies of CO₂ adsorbed in these MOFs. Then, in the next step, we use vdW-DF2 to calculate the corresponding shifts and determine the mechanisms that cause them. Unlike in experiments, first-principles simulations allow us to artificially freeze different degrees of freedom of the system, enabling us to understand the importance of different physical contributions to the CO₂ frequency shifts. By analyzing the CO₂ asymmetric stretch frequency under different geometries, we identify three different factors determining the frequency shift of physisorbed CO₂, namely, the length of the molecule, the asymmetric distortion, and the metal center.

II. METHOD

A. Metal organic framework synthesis

Mg-MOF74,²⁸ Zn-MOF74,²⁹ Co-MOF74,³⁰ and Ni-MOF74⁷ were synthesized according to procedures described in the literature;^{9,23}

Mg-MOF74: 2,5-Dihydroxyterephthalic acid (H₂DHBDC) (99 mg, 0.5 mmol) and Mg(NO₃)₂·6H₂O (257 mg, 1.0 mmol) were dissolved in the mixture of THF (7 mL), 1M NaOH solution (2 mL), and water (3 mL) with stirring. The mixture was then sealed in a Teflon-lined autoclave and heated at 110°C for 3 days. The product was collected by filtration as a light-yellow substance. Yield: 115 mg, 83%.

Zn-MOF74: The preparation of Zn-MOF74 was similar to that of Mg-MOF74 except that Zn(NO₃)₂·6H₂O (298 mg, 1.0 mmol) was used instead of Mg(NO₃)₂·6H₂O. Yield: 160 mg, 87%.

Co-MOF74: H₂DHBDC (150 mg, 0.75 mmol) and [Co(NO₃)₂]·6H₂O (186 mg, 0.75 mmol) were dissolved in 15 mL of THF-H₂O solution (50:50, v:v) with stirring. The mixture was transferred to a Teflon-lined autoclave, which was then sealed and heated at 110°C for 3 days. Brown-red rod-shape crystals were isolated by filtration and dried under vacuum. Yield: 130 mg, 50%.

Ni-MOF74: A mixture of H₂DHBDC (60 mg, 0.3 mmol), [Ni(NO₃)₂]·6H₂O (174 mg, 0.6 mmol), DMF (9 mL), and H₂O (1 mL) was transferred to a Teflon-lined autoclave and heated in an oven at 100°C for 3 days. Brown crystalline powder was collected by filtration and dried under vacuum. Yield: 75 mg, 72%.

All as-synthesized materials were exchanged with fresh methanol four times in a duration of 4 days, followed by drying in a vacuum oven at room temperature, and annealing at 480 K overnight under high vacuum before spectroscopic measurements.

B. IR and Raman spectroscopy

IR absorption spectroscopy of CO₂ adsorption in the MOFs was performed in transmission at room temperature using a liquid-N₂-cooled InSb detector. Approximately 12 mg of MOF powder was pressed on a KBr support and mounted in a high-temperature high-pressure cell (Specac product P/N 5850c) and heated to 200°C in vacuum (100 mTorr) overnight for complete desolvation. MOF74 samples were activated by solvent exchange in methanol and drying in vacuum at room temperature. Subtraction of the gas phase CO₂ contribution to the IR spectra was performed as described in Ref. 11.

Raman spectroscopy measurements were performed using a solid state 532 nm laser. The activated sample was loaded into a Linkam FTIR cooling/heating stage, and the sample was heated to 120°C in vacuum (900 mTorr) for complete dehydration. A laser power of 0.113–1.23 mWatt was used to avoid sample burning from the laser.

C. First-principles calculations

For our first-principles calculations we used DFT as implemented in *ABINIT*,^{38,39} utilizing vdW-DF2 to describe exchange and correlation effects.³¹ Troulier-Martin type norm-conserving pseudopotentials and a plane-wave basis are used,⁴⁰ where the Zn 3*d* semicore electrons are also considered as valence electrons. To ensure a full convergence of the structure and energy, a kinetic energy cutoff of 45 Hartree is used for the plane-wave basis. For structural relaxation, we start from the experimental atomic positions and relax them using vdW-DF2 until the force on each atom is less than 0.05 eV/Å. The unit cell parameters are fixed to the experimental values, where for the hexagonal unit cell $a = 25.881$ Å and $c = 6.8789$ Å for Mg-MOF74²⁵ and $a = 25.887$ Å and $c = 6.816$ Å for Zn-MOF74,⁶ respectively.

Due to the complex interaction between CO₂ and MOF74, many local minimum energy sites exist, making it difficult to identify the low-energy adsorption site, which corresponds to the low pressure absorption. Indeed, multiple adsorption sites and binding energies are determined from our simulations. In this work, we performed calculations with multiple initial positions and orientations of CO₂ relative to the MOF74, and choose the site with the lowest total energy as the one for our analysis. To guarantee that CO₂ is adsorbed at the equivalent lowest energy site in both Mg-MOF74 and Zn-MOF74, we start the atomic position relaxation of CO₂ in Mg-MOF74 with the coordinates of the relaxed CO₂ in Zn-MOF74, which is possible due to the isostructure and symmetry of the two MOF systems. This ensures that we are comparing the effect of the open metal site on CO₂ in the two different systems on the same footing.

To calculate the frequency shifts we use a frozen-phonon approach in the CO₂ molecules, where the

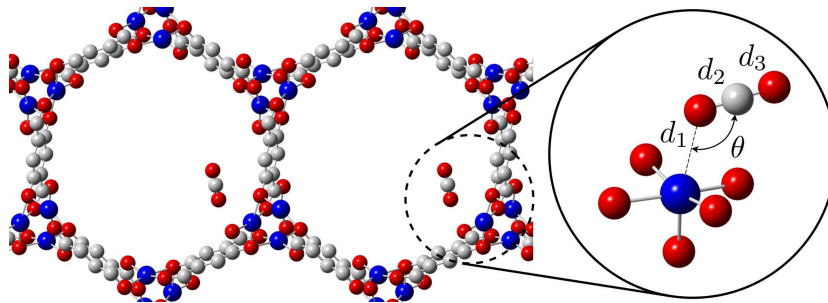


FIG. 1. (Color online) Illustration figure of CO_2 adsorbed in Zn-MOF74. Calculated values of d_1 , d_2 , d_3 , and θ for CO_2 in Zn-MOF74 and Mg-MOF74 can be found in Table I.

TABLE I. Calculated binding energy ΔE (kJ/mol), angle θ (deg), and various distances d_i and l (\AA) (where $l = d_2 + d_3$) of the CO_2 molecule physisorbed in the MOF; see Fig. 1 for further details. The calculated free CO_2 parameters are $d_0 = 1.1630 \text{ \AA}$ and $l_0 = 2.3260 \text{ \AA}$.

MOF	ΔE	θ	d_1	$d_2 - d_0$	$d_3 - d_0$	$l - l_0$
Mg-MOF74	35.4	120.8	2.53	+0.0062	-0.0059	+0.0003
Zn-MOF74	26.9	116.4	2.69	+0.0048	-0.0039	+0.0009

MOF74 atoms are kept fixed, while each of the atoms in the CO_2 is distorted in $\pm dx, \pm dy, \pm dz$ directions by small distortions $\Delta r = 0.02 \text{ \AA}$, to calculate the force on each atom. The symmetrized force matrix $2F(\Delta r) = F(\Delta r) - F(-\Delta r)$ is constructed for only the atoms within the CO_2 molecule, based on the approximation that the interaction between the CO_2 molecule and the MOF is weak and thus the effect of the vibration of the MOF74 atoms on the CO_2 frequencies are negligible. However, notice that, while the MOF74 atoms are kept fixed, the van der Waals forces experienced by the CO_2 due to the presence of the MOF74 are included by our vdW-DF2 calculation. To evaluate the effects of the surrounding MOF lattice, tests have been performed to allow vibrations of several MOF74 atoms in the vicinity of the adsorbed CO_2 molecule; frozen phonon calculations with such an extended force matrix show no observable effect on the CO_2 frequencies. In general, our studies show that calculated frequencies are converged to within less than 1 cm^{-1} .

III. RESULTS AND DISCUSSION

A. Structure and binding energy

The structure of CO_2 adsorbed in MOF74 is illustrated in Fig. 1. In this work, we consider only CO_2 adsorption under low pressure smaller than 7 Torr, where the open metal site in MOF74 is far from fully occupied. In our first-principles simulations one CO_2 per six metal sites adsorption is considered, corresponding to

the low-loading situation observed experimentally. For the binding energy of CO_2 adsorbed in Mg-MOF74, we find 35.4 kJ/mol , while it binds somewhat weaker in Zn-MOF74 with 26.9 kJ/mol . Comparing the distance of the CO_2 molecules with the open metal site, we find a metal-oxygen distance (d_1 in Fig. 1) of 2.53 \AA for Mg versus 2.69 \AA for Zn. In other words, CO_2 binds stronger and closer to the metal center in Mg-MOF74 than it does in Zn-MOF74. At the same time, similar metal- CO_2 angles ensure that the CO_2 is adsorbed at equivalent sites in both MOFs, with slightly different metal- CO_2 angles of 120.8° and 116.4° in Mg-MOF74 and Zn-MOF74, respectively.

Further analyzing the structure of the adsorbed CO_2 molecule, we see that the C=O bond closer to the metal site (d_2 in Fig. 1) is elongated in both systems with a value of 1.1692 \AA in Mg-MOF74 and 1.1678 \AA in Zn-MOF74; in free CO_2 it is 1.1630 \AA (denoted as d_0 in Table I). On the other hand, the C=O bond farther away from the metal center (d_3 in Fig. 1) are both shortened, with a value 1.1571 \AA in Mg-MOF74 and 1.1591 \AA in Zn-MOF74. A summary of distortions is shown in Table I. This distortion can be understood intuitively via the interaction between the CO_2 and the metal center, where the attraction from the metal center weakens (and thus elongates) the nearby C=O bond, shortening the remaining C=O bond. By comparing with the free CO_2 value of 1.1630 \AA , we see that the CO_2 asymmetric distortion in Mg-MOF74 is stronger than in Zn-MOF74. Summing up the two C=O bonds yields the overall length of the CO_2 molecule, which shows an elongation of $+0.0003 \text{ \AA}$ and $+0.0009 \text{ \AA}$ for Mg-MOF74 and Zn-MOF74 adsorption, as shown in Table I. It has been reported previously that CO_2 molecules adsorbed in the MOF structure might experience some nonlinear distortion, i.e., an O-C-O angle differing from 180° . In this work, we also allow nonlinear distortion of the CO_2 molecule, and we find that the relaxed CO_2 molecule are only slightly bent after adsorbed within MOF74, featuring an O-C-O angle of 179.25° in Zn-MOF74 and 178.97° in Mg-MOF74.

As mentioned above, multiple local minimum adsorption sites are obtained during the relaxation of CO_2 within the MOF74, leading to different metal- CO_2 dis-

tances and binding energies. For instance, in Zn-MOF74 positions with similar location but Zn-CO₂ distances of 2.96 Å and 3.09 Å are found with binding energies of 25.6 kJ/mol and 24.8 kJ/mol, respectively. In addition to these sites similar to the global minimum metal site, we also find a secondary non-metal site for CO₂ absorption, which lies between two neighboring equivalent metal sites along the direction of the MOF74 pore, with a distance of 3.99 Å to the nearest metal Zn site and a binding energy of 21.8 kJ/mol—clearly much smaller than at the metal site. The distance between two equivalent metal sites along the pore direction in MOF74 is the *c* length of the hexagonal unit cell, which is approximately 6.8 Å, as mentioned above. It is thus possible that at high CO₂ pressure, when all the metal sites are occupied (1 CO₂ per 1 metal), more CO₂ can still be absorbed within the MOF74 occupying the secondary site, with a CO₂-CO₂ distance of approximately 3.4 Å along the pore direction, thus resulting in a higher (2 CO₂ per 1 metal) storage density of CO₂ within MOF74.

B. CO₂ frequencies from experiment

IR absorption spectra of CO₂ absorbed in Mg-MOF74 and Zn-MOF74 are shown in Fig. 2, depicting a main IR absorption band attributed to the asymmetric stretch of CO₂ at 2338 and 2352 cm⁻¹ for Zn-MOF74 and Mg-MOF74. The integrated areas of the IR band of the asymmetric CO₂ stretch mode can serve as an indication of the relative amount of CO₂ absorbed in MOF74. Figure 3 summarizes the integrated area as a function of CO₂ pressure for both Mg-MOF74 and Zn-MOF74, showing that under the same pressure, the amount of absorbed CO₂ is more for the case of Mg-MOF74 than it is for Zn-MOF74. These results are consistent with isotherm measurements of CO₂ reported in Ref. 7. Similar IR measurements are also performed on Co-MOF74 and Ni-MOF74, showing shifts of the asymmetric CO₂ stretch (~ 2340 cm⁻¹) similar to that in Zn-MOF74.

In Fig. 2, the shoulder peaks at 2325 and 2341 cm⁻¹ are attributed to the combination mode of the stretch mode and the two non-degenerate bending modes (denoted as δ_1 and δ_2 in Fig. 2). Experimentally, it is difficult to identify the bending modes in the low frequency range because of their weak intensity as compared to the MOF vibrations. Therefore, we could only resolve one of these non-degenerate bending modes at ~ 658 cm⁻¹. The similarity of the bending mode for the Mg and Zn cases is consistent with the close calculated values for both systems shown in Table II.

Raman spectroscopy measurements were performed to find the experimental value of the symmetric stretch mode of absorbed CO₂ for the Co-MOF74 and Ni-MOF74. The symmetric stretch was found to be approximately -1380 and -1382 cm⁻¹ for Co-MOF74 and Ni-MOF74, respectively. Because of the strong MOF Raman modes, the symmetric stretch for Mg-MOF74 and

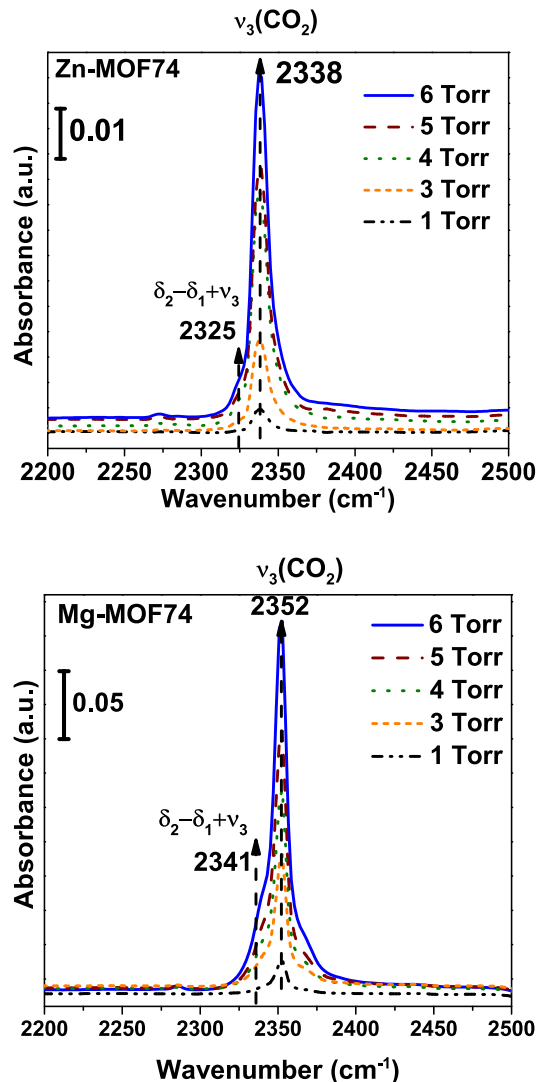


FIG. 2. IR absorption spectra of CO₂ absorbed into Zn-MOF74 (top) and in Mg-MOF74 (bottom) at changing CO₂ pressure (1–6 Torr).

Zn-MOF74 is not available. A summary of the IR and Raman data for the frequencies of the absorbed CO₂ within MOF74 can be found in Table II.

C. Analyzing the frequency shift

When we consider the frequency shifts from the free CO₂ situation, comparing with 2349 cm⁻¹ for free CO₂, the asymmetric stretch for CO₂ absorbed in MOF74 has been shifted by +3 and -11 cm⁻¹ for Mg and Zn-MOF74, respectively. Our first-principles frozen-phonon calculations are in good agreement with this result and we find the CO₂ asymmetric stretch mode experiences a slight redshift of approximately -0.5 cm⁻¹ in Mg-MOF74 and -8.1 cm⁻¹ in Zn-MOF74. Furthermore, the bending modes calculated also experience redshifts of about

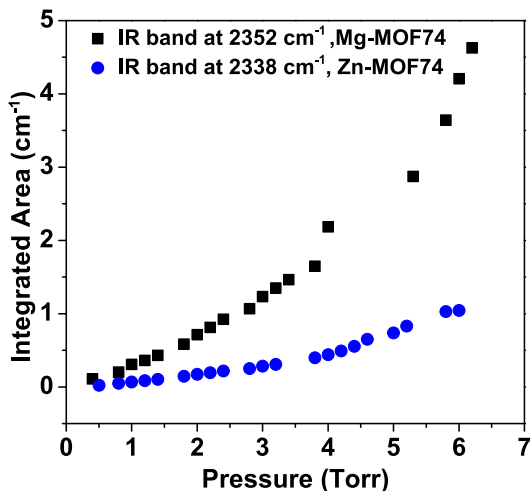


FIG. 3. Integrated areas of IR absorption peaks for the asymmetric stretch modes for CO₂ adsorbed in Mg-MOF74 and Zn-MOF74 as a function of CO₂ pressure.

-10 cm⁻¹ in both Mg-MOF74 and Zn-MOF74, which is in excellent agreement with the experimentally observed -9 cm⁻¹ redshifts in these systems. The calculated results for all the CO₂ modes are summarized in Table II.

We have shown above that CO₂ is binding stronger in Mg-MOF74, with a closer metal-CO₂ distance and larger molecule distortions. It is thus puzzling to observe that the ν_3 frequency shift for CO₂ in Mg-MOF74 is much smaller compared with that in Zn-MOF74. There have been many experiments and theoretical simulations studying the frequency shifts of small molecules adsorbed in MOFs, such as H₂, CO₂, CO, etc.^{8-13,19-24} It is well known that the frequency shift of small molecule vibrations has no obvious correlations with either the binding energy or the adsorption site of the molecule within the MOF. In our example here with iso-structural Mg-MOF74 and Zn-MOF74, this behavior is even more obvious, as Mg and Zn have similar electronic structures: the metal centers have valence electrons of 3s and 4s, respectively, except that Zn has the additional fully occupied 3d orbital electrons. Thus the question arises as to what the physical reason is that determines the frequency shift of the small molecules adsorbed in the MOF.

Several reasons may contribute to the frequency shift. For instance, by analyzing the geometries of the adsorbed CO₂, we noticed that the adsorbed CO₂ molecules have been distorted from their free molecule geometry, exhibiting an off-center shift of the carbon atom, as well as an elongated overall length of the molecule, as summarized in Table I (The slight nonlinear distortion of the CO₂ molecule is ignored here in this analysis). The change in the length of the molecule and the asymmetric distortion can both affect the vibrational frequencies. Beyond the effect of the change in the molecule geometry, the nearby open metal center might also play a direct role in the frequency shift, by attracting or repelling the nearby oxygen atom in the CO₂ molecules during the vibration.

TABLE II. Vibrational frequencies (cm⁻¹) of CO₂ physisorbed in MOF74. Higher accuracy is kept for the calculated ν_3 for further detailed analysis.

	system	sym. ν_1	bend ν_2	asym. ν_3
	free CO ₂ [†]	1388	667	2349
	Mg-MOF74	—	658	2352
exp.	Zn-MOF74	—	658	2338
	Co-MOF74	1380	—	2340
	Ni-MOF74	1382	—	2340
	free CO ₂	1298	646, 639	2288.5
calc.	Mg-MOF74	1294	636, 630	2288.0
	Zn-MOF74	1296	637, 632	2280.4

[†]Taken from Ref. 41.

To understand these different contributions, in the following we analyze the influences of each of these factors on the frequency of the CO₂ vibrations separately and summarize their contributions in Table III.

1. Change in molecule length

We first analyze the effect of the changing molecule length. To do this, we perform frozen-phonon calculations on the free CO₂ molecules fixed to the lengths of the CO₂ adsorbed in Mg-MOF (shown in the last column of Table I), while keeping the carbon atom at the center of the molecule. With this geometry, the CO₂ asymmetric stretch is shifted by -1.6 cm⁻¹. A similar calculation by setting the CO₂ molecule length to the value of that adsorbed in Zn-MOF74 yields a redshift in ν_3 of -3.7 cm⁻¹. Note that overall the CO₂ in Mg-MOF74 is elongated by 0.0003 Å, while that in Zn-MOF74 is elongated by 0.0009 Å. The CO₂ with the longer length (in Zn-MOF74) has a larger redshift of approximately -2.1 cm⁻¹ than that in Mg-MOF74. That is, a longer molecule has more redshift, as suggested by common sense.

2. Asymmetric distortion of the molecule

Next, we take the asymmetric effect into consideration by placing the CO₂ at exactly the same geometries as they are in the two MOFs, while removing the surrounding MOFs. The frequency shift thus comes from the change in both the length of the CO₂ molecule and the asymmetric shift of the carbon atom. Our frozen-phonon calculations give an overall frequency shift of -0.5 and -3.0 cm⁻¹ for the ν_3 mode of CO₂ from Mg-MOF74 and Zn-MOF74, respectively. Subtracting the previous results of only considering the length of the molecule, the asymmetric distortion of the carbon atom causes a slight blue shift in the asymmetric stretch with a value of 1.1 and 0.7 cm⁻¹ in Mg-MOF74 and Zn-MOF74.

To confirm these results, we also perform calculations using another setup, where we keep the optimized CO_2 within the MOF and shift the carbon atom to the center of the CO_2 molecule. In this way, we include the effect of the MOF environment and the length effect. The only difference between this new setup and the optimized CO_2 in MOFs is that the carbon atom off-center asymmetric effects are eliminated. Our simulations show that the CO_2 in such a geometry has a frequency shift of -1.7 and -8.7 cm^{-1} in Mg-MOF74 and Zn-MOF74. Comparing these results with the frequency shifts for relaxed CO_2 in the same MOFs, we find similar differences of approximately 1.2 and 0.6 cm^{-1} for the case of Mg-MOF74 and Zn-MOF74, which are consistent with our previous results. It is thus clear that the carbon off-center distortion indeed causes slight blue shifts in the ν_3 frequency. This result can also be understood in the following way: by shifting the carbon atom off-center, the CO_2 atom is distorted asymmetrically in a similar pattern as the asymmetric stretch mode, which thus favors the asymmetric stretch. As shown in Table I, the asymmetric distortion in Mg-MOF74 is stronger than that in Zn-MOF74, which is consistent with a larger blueshift effect in the $\text{CO}_2 \nu_3$ frequency.

3. Effect of the metal center

By comparing with the results for optimized CO_2 in the MOFs, the previous results of the effects of the CO_2 molecule geometry change on the ν_3 frequency shifts yield the influence of the metal center on the ν_3 frequencies. A direct comparison gives a frequency shift of -5.1 cm^{-1} for the Zn-MOF74 and 0 cm^{-1} for Mg-MOF74. This result is quite a surprise, claiming that the open Zn center has a strong redshift influence on the ν_3 frequency, while the Mg center has no effect at all.

To confirm this result, we place the undistorted CO_2 molecule at the same position and angle of the adsorption site, with the position of the oxygen atom near the metal center fixed, while the positions of the carbon and the other oxygen atom shifted slightly along the line to achieve the free CO_2 geometry. The frequency shift of the CO_2 asymmetric stretch thus results mostly from the direct effect of the metal center. With this geometry, our calculation shows that, while the asymmetric stretch of CO_2 in Zn-MOF74 is shifted by approximately -5.0 cm^{-1} , the one in Mg-MOF74 has a negligible shift of about -0.6 cm^{-1} , confirming our previous results. In other words, the fact that the oxygen atom in CO_2 is being close to the open metal center has a significantly different effect depending on the metal atoms. While the Zn atom affects the frequency strongly, the Mg atom has almost no effect at all. This result is quite striking, since the metal centers Mg and Zn have a very similar valence electronic structure with $3s$ and $4s$ electrons as the outermost valence states. The result thus shows that fully occupied semicore $3d$ electrons in Zn have an im-

TABLE III. Frequency shifts of ν_3 (cm^{-1}) for different geometries. See main text for details about these geometry.

effect	Mg-MOF74	Zn-MOF74
length	-1.6	-3.7
length+asym	-0.5	-3.0
length+metal	-1.7	-8.7
metal	-0.6	-5.0
overall	-0.5	-8.1

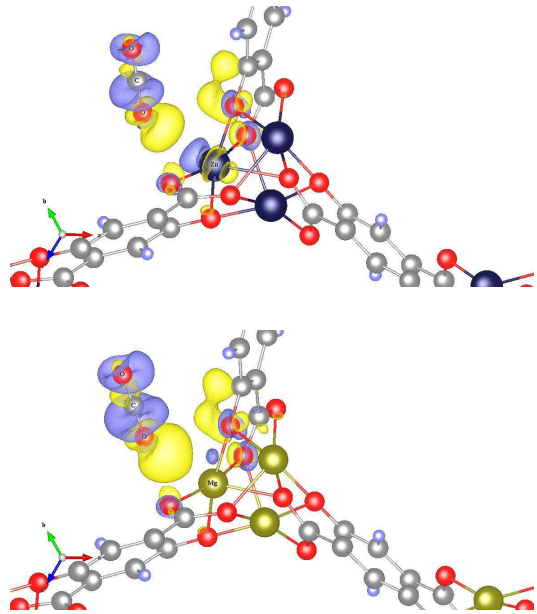


FIG. 4. (Color online) Charge density differences $\Delta\rho = \rho_{\text{MOF74}+\text{CO}_2} - \rho_{\text{MOF74}} - \rho_{\text{CO}_2}$ from before and after CO_2 adsorbed into Zn-MOF74 (top) and in Mg-MOF74 (bottom).

portant effect in the interaction with the adsorbed CO_2 molecules. In fact, in Co-MOF74 and Ni-MOF74 where $3d$ electrons are also present in the metal center, experimentally we observed that the asymmetric stretch of CO_2 has been similarly red-shifted by -10 cm^{-1} as that in Zn-MOF74, as summarized in Table II, indicating that the $3d$ orbitals are indeed playing a similar role for the CO_2 frequencies in these MOF74 systems.

The contributions of these three effects to the ν_3 frequency shifts are summarized in Table III.

D. Microscopic insight and implication of bonding

In order to gain more insight understanding for the differences in the interaction between CO_2 and the two different MOF74s, we investigate the charge density differences before and after CO_2 adsorbed inside the MOF74. To do this, we calculate the charge densities of the CO_2 and MOF74 separately, by removing CO_2 from the MOF74, while keeping the atomic positions. The charge

density difference is defined by

$$\Delta\rho = \rho_{\text{MOF74+CO}_2} - \rho_{\text{MOF74}} - \rho_{\text{CO}_2}.$$

The charge density difference $\Delta\rho$ thus illustrates the effect of the interaction by placing the CO_2 inside the MOF74. The obtained charge density differences are plotted in Fig. 4.

Not surprisingly, by introducing CO_2 inside the MOF74, the electrons in CO_2 are attracted toward the metal side, featuring electron deficiency in the far end (light blue color) and electron gaining near the metal site (yellow color). This can be understood via the attraction from the positively charged metal centers, similar for both Mg and Zn centers. However, one can also observe differences between the Zn-MOF74 and Mg-MOF74 systems, where the electron transfers more in the later than the former. As we look at the metal center, we can observe that near Zn atom, the electrons shift slightly away from the CO_2 adsorption position. This charge density change near the Zn centers are missing from those Mg center, clearly showing that it is an effect of the d -orbitals of the Zn atoms. It is thus clear that the presence of the d -orbitals prevents the charge density transfer within the adsorbed CO_2 molecules, leading to smaller charge transfer as compared with those near Mg center. As a result, the bonding energy between CO_2 and Zn-MOF74 is smaller than that of CO_2 in Mg-MOF74. On the other hand, this clear effect of the Zn d -orbital effectively affect the IR frequency shift of the adsorbed CO_2 molecule, leading to the differences between the two systems as we discussed above.

E. Discussion

From the previous analysis, it is now clear that the ν_3 frequency shifts of the CO_2 adsorbed in MOF74 can be understood by the three distinct contributions, namely, the change of the molecule length, the off-center asymmetric distortion, and the direct effect of the open metal site. The interaction between CO_2 and the MOF causes distortions in the molecule geometry, which affect the vibration modes. The adsorbed CO_2 molecules experience a stronger asymmetric distortion in Mg-MOF74, as shown in Table I, which is consistent with the larger bonding energy calculated, as well as the larger integrated area for the asymmetric stretch IR peak. However, such an asymmetric distortion only has a small effect on the ν_3 frequency shifts. On the other hand, although CO_2 is less asymmetrically distorted in Zn-MOF74, it experiences a larger elongation in the overall length, which affects the ν_3 frequency shift more strongly. In addition, the nearby open metal site can play a quite different role in affecting the CO_2 vibrations, where in this work, the Zn affects strongly while Mg has barely any effect on the ν_3 frequency shift. The differences between these two MOF74 can be intuitively understood by the presence of the d -orbitals within the Zn atoms and the missing

of those within Mg centers, as illustrated in the charge density difference plots.

The results of this work provide insight to the factors that determine the frequency shifts of the adsorbed CO_2 in MOF, helping to understand the puzzling frequency shifts observed experimentally. More importantly, the analysis method of this work can serve as a new way to understand the more widely examined molecule-MOF interactions and frequency shifts. However, one must keep in mind that frequency shifts obtained through such fixed geometries and environments reflect the influence of different factors on the force matrix and can only give an estimation of the influence of certain factors. In reality, originating in the molecule-MOF interaction, all three factors are closely connected intrinsically and it is impossible to exactly separate these different effects.

IV. SUMMARY

In this work, we analyzed the physics determining the asymmetric frequency shift of the CO_2 molecules physisorbed in MOFs. Our specific findings are summarized as follows: (i) first-principles vdW-DF2 simulations determine that the CO_2 's have a closer distance to the Mg center and a larger binding energy within Mg-MOF74 comparing with those in Zn-MOF74. (ii) Contrary to our intuition, and despite the isostructure and the similarity of the open metals Mg and Zn, the asymmetric stretch frequency of physisorbed CO_2 has been shifted stronger in Zn-MOF74 (-11 cm^{-1} by IR and -8.1 cm^{-1} by theory) than that in Mg-MOF74 ($+3 \text{ cm}^{-1}$ by IR and -0.5 cm^{-1} by theory). (iii) By comparing the response in two isostructure MOFs, namely Zn-MOF74 and Mg-MOF74, we identified the three most important factors contributing to the frequency shifts: the elongated CO_2 molecule, the off-center asymmetric distortion of the carbon atoms, and the effect of the metal center. (iv) The asymmetric stretch frequency is very sensitive to the overall length of the CO_2 molecule. Adsorbed in the MOF, the CO_2 molecules are elongated, which leads to a redshift in the frequency. This elongation effect and resulting redshift are more significant for CO_2 adsorbed in Zn-MOF74 compared with those in Mg-MOF74. (v) The slight off-center asymmetric distortion, on the other hand, favors the asymmetric stretch and causes a slight blueshift in the frequency. (vi) Aside from changing the geometries of the CO_2 molecule (i.e. elongating the molecule, causing off-center asymmetric distortion of the carbon atom) and depending on the species of the open metal site, the direct interaction of the oxygen atom with the metal center can have very different effects on the frequency of the asymmetric stretch, where the Zn center leads to a redshift of about -5 cm^{-1} and the Mg center has a negligible effect on the frequency. (vii) The observed different effects of the Zn-MOF74 and Mg-MOF74 can be understood by the presence of d -orbital electrons in the Zn-MOF74.

ACKNOWLEDGMENTS

We would like to thank David Langreth, the father of vdW-DF, for his inspirational research. We thank Pro-

fessors K. Rabe and D. Vanderbilt for very helpful discussions throughout the whole project. This work was supported in full by the Department of Energy Grant, Office of Basic Energy Sciences, Materials Sciences and Engineering Division, Grant No. DE-FG02-08ER46491.

-
- ¹ R. Banerjee, A. Phan, B. Wang, C. Knobler, H. Furukawa, M. ÓKeeffe, and O. M. Yaghi, *Science* **319**, 939 (2008).
² R. E. Morris, *Nat. Chem.* **3**, 347 (2011).
³ D. S. Sholl, *Nature Chemistry* **3**, 429 (2011).
⁴ N. L. Rosi, J. Kim, M. Eddaoudi, B. Chen, M. ÓKeeffe, and O. M. Yaghi, *J. Am. Chem. Soc.* **127**, 1504 (2005).
⁵ J. L. C. Rowsell and O. M. Yaghi, *J. Am. Chem. Soc.* **128**, 1304 (2006).
⁶ Y. Liu, H. Kabbour, C. M. Brown, D. A. Neumann, and C. C. Ahn, *Langmuir* **24**, 4772 (2008).
⁷ S. R. Caskey, A. G. Wong-Foy, and A. J. Matzger, *J. Am. Chem. Soc.* **130**, 10870 (2008).
⁸ H. Wu, J. M. Simmons, G. Srinivas, W. Zhou, and T. Yildirim, *J. Phys. Chem. Lett.* **1**, 1946 (2010).
⁹ N. Nour, J. F. Veyan, L. Kong, H. Wu, Y. Zhao, J. Li, D. C. Langreth, and Y. J. Chabal, *J. Am. Chem. Soc.* **132**, 14834 (2010).
¹⁰ L. Valenzano, B. Civalleri, S. Chavan, G. T. Palomino, C. O. Areán, and S. Bordiga, *J. Phys. Chem. C* **114**, 11185 (2010).
¹¹ N. Nour, P. Thissen, Y. Yao, R. C. Longo, K. Roodenko, H. Wu, Y. Zhao, K. Cho, J. Li, D. C. Langreth, and Y. J. Chabal, *J. Am. Chem. Soc.* **133**, 12849 (2011).
¹² L. Kong, Y. J. Chabal, and D. C. Langreth, *Phys. Rev. B* **83**, 121402(R) (2011).
¹³ L. Kong, V. R. Cooper, N. Nijem, K. Li, J. Li, Y. J. Chabal, and D. C. Langreth, *Phys. Rev. B* **79**, 081407(R) (2009).
¹⁴ H. Wu, W. Zhou, and T. Yildirim, *J. Am. Chem. Soc.* **131**, 4995 (2009).
¹⁵ W. Zhou and T. Yildirim, *J. Phys. Chem. C* **112**, 8132 (2008).
¹⁶ S. Xiang, W. Zhou, Z. Zhang, M. A. Green, Y. Liu, and B. Chen, *Angew. Chem.* **122**, 4719 (2010).
¹⁷ Y. Y. Sun, Y. Kim, and S. B. Zhang, *J. Am. Chem. Soc.* **129**, 12606 (2007).
¹⁸ H. C. Hoffmann, B. Assfour, F. Epperlein, N. Klein, S. Paasch, I. Senkowska, S. Kaskel, G. Seifert, and E. Brunner, *J. Am. Chem. Soc.* **133**, 8681 (2011).
¹⁹ K. Sumida, C. M. Brown, Z. R. Herm, S. Chavan, S. Bordiga, and J. R. Long, *Chem. Commun.* **47**, 1157 (2011).
²⁰ P. D. C. Dietzel, R. E. Johnsen, H. Fjellvåg, S. Bordiga, E. Groppo, S. Chavan, and R. Blom, *Chem. Commun.* **41**, 5125 (2008).
²¹ S. Chaven, F. Bonino, J. G. Vitillo, E. Groppo, C. Lamberti, P. D. C. Dietzel, A. Zecchina, and S. Bordiga, *Phys. Chem. Chem. Phys.* **11**, 9811 (2009).
²² S. A. FitzGerald, J. Hopkins, B. Burkholder, M. Friedman, and J. L. C. Rowsell, *Phys. Rev. B* **81**, 104305 (2010).
²³ N. Nijem, L. Kong, Y. Zhao, H. Wu, J. Li, D. C. Langreth, and Y. J. Chabal, *J. Am. Chem. Soc.* **133** 4782 (2011).
²⁴ S. A. FitzGerald, K. Allen, P. Landerman, J. Hopkins, J. Matters, R. Myers, and J. L. C. Rowsell, *Phys. Rev. B* **77**, 224301 (2008).
²⁵ H. Wu, W. Zhou and T. Yildirim, *J. Am. Chem. Soc.* **131**, 4995 (2009).
²⁶ W. Zhou, H. Wu, and T. Yildirim, *J. Am. Chem. Soc.* **130**, 15268 (2008).
²⁷ J. T. Hughes and A. Navrotsky, *J. Am. Chem. Soc.* **133**, 9184 (2011).
²⁸ P. D. C. Dietzel and R. Blom, H. Fjellvåg, *Eur. J. Inorg. Chem* **2008**, 3624 (2008).
²⁹ P. D. C. Dietzel, R. E. Johnsen, R. Blom, and H. Fjellvåg, *Chem. Eur. J.* **14**, 2389 (2008).
³⁰ P. D. C. Dietzel, Y. Morita, R. Blom, and H. Fjellvåg, *Angew. Chem. Int. Ed.* **44**, 6354 (2005).
³¹ K. Lee, É. D. Murray, L. Kong, B. I. Lundqvist, and D. C. Langreth, *Phys. Rev. B* **82**, 081101(R) (2010).
³² M. Dion, H. Rydberg, E. Schröder, D. C. Langreth, and B. I. Lundqvist, *Phys. Rev. Lett.* **92**, 246401 (2004); **95**, 109902 (2005).
³³ T. Thonhauser, V. R. Cooper, Li Shen, A. Puzder, P. Hyldgaard, and D. C. Langreth, *Phys. Rev. B* **76**, 125112 (2007).
³⁴ D. C. Langreth et al., *J. Phys.: Condens. Matter* **21**, 084203 (2009).
³⁵ T. Thonhauser, A. Puzder, and D.C. Langreth, *J. Chem. Phys.* **124**, 164106 (2006); S. Li, V.R. Cooper, T. Thonhauser, A. Puzder, and D. C. Langreth, *J. Phys. Chem. A* **112**, 9031 (2008); J. Hooper, V. R. Cooper, T. Thonhauser, N. A. Romero, F. Zerilli, and D. C. Langreth, *ChemPhysChem* **9**, 891 (2008).
³⁶ M. Mura, A. Gulans, T. Thonhauser, and L. Kantorovich, *Phys. Chem. Chem. Phys.* **12**, 4759 (2010).
³⁷ V. R. Cooper, T. Thonhauser, A. Puzder, E. Schröder, B. I. Lundqvist, and D. C. Langreth, *J. Am. Chem. Soc.* **130**, 1304 (2008); V. R. Cooper, T. Thonhauser, and D. C. Langreth, *J. Chem. Phys.* **128**, 204102 (2008); S. Li, V. R. Cooper, T. Thonhauser, B. I. Lundqvist, and D. C. Langreth, *J. Phys. Chem. B* **113**, 11166 (2009).
³⁸ X. Gonze, B. Amadon, P.-M. Anglade, J.-M. Beuken, F. Bottin, P. Boulanger, F. Bruneval, D. Caliste, R. Caracas, M. Cote, T. Deutsch, L. Genovese, Ph. Ghosez, M. Giantomassi, S. Goedecker, D.R. Hamann, P. Hermet, F. Jollet, G. Jomard, S. Leroux, M. Mancini, S. Mazevet, M.J.T. Oliveira, G. Onida, Y. Pouillon, T. Rangel, G.-M. Rignanese, D. Sangalli, R. Shaltaf, M. Torrent, M.J. Verstraete, G. Zerah, J.W. Zwanziger, *Computer Phys. Commun.* **180**, 2582 (2009).
³⁹ X. Gonze, G.-M. Rignanese, M. Verstraete, J.-M. Beuken, Y. Pouillon, R. Caracas, F. Jollet, M. Torrent, G. Zerah, M. Mikami, Ph. Ghosez, M. Veithen, J.-Y. Raty, V. Olevano, F. Bruneval, L. Reining, R. Godby, G. Onida, D.R. Hamann, and D. C. Allan, *Zeit. Kristallogr.* **220**, 558 (2005).
⁴⁰ N. Troullier and J. L. Martins, *Phys. Rev. B* **43**, 1993 (1991).

⁴¹ NIST Standard Reference Database 69: Nist Chemistry
WebBook at <http://webbook.nist.gov/chemistry>.